PET imaging of microglia by targeting macrophage colony-stimulating factor 1 receptor (CSF1R)

Andrew G. Horti[a,1], Ravi Naik[a], Catherine A. Foss[a], Il Minn[a], Varia Misheneva[b], Yong Du[a], Yuchuan Wang[c], William B. Mathews[a], Yunkou Wu[a], Andrew Hall[a], Catherine LaCourse[b], Hye-Hyun Ahn[a], Hwanhee Nam[a], Wojciech G. Lesniak[a], Heather Valentine[a], Olga Pletnikova[d], Juan C. Troncoso[d,e], Matthew D. Smith[e], Peter A. Calabresi[e], Alena V. Savonenko[d], Robert F. Dannals[a], Mikhail V. Pletnikov[b], and Martin G. Pomper[a,b,1]

[a]Russell H. Morgan Department of Radiology and Radiological Science, The Johns Hopkins University School of Medicine, Baltimore, MD 21287; [b]Department of Psychiatry, The Johns Hopkins University School of Medicine, Baltimore, MD 21287; [c]Merck & Co., Inc., West Point, PA 19486; [d]Department of Pathology, The Johns Hopkins University School of Medicine, Baltimore, MD 21287; and [e]Department of Neurology, The Johns Hopkins University School of Medicine, Baltimore, MD 21287

Edited by Jason S. Lewis, Memorial Sloan Kettering Cancer Center, New York, NY, and accepted by Editorial Board Member Carl F. Nathan December 10, 2018 (received for review July 16, 2018)

While neuroinflammation is an evolving concept and the cells involved and their functions are being defined, microglia are understood to be a key cellular mediator of brain injury and repair. The ability to measure microglial activity specifically and noninvasively would be a boon to the study of neuroinflammation, which is involved in a wide variety of neuropsychiatric disorders including traumatic brain injury, demyelinating disease, Alzheimer's disease (AD), and Parkinson's disease, among others. We have developed [^{11}C]CPPC [5-cyano-*N*-(4-(4-[^{11}C]methylpiperazin-1-yl)-2-(piperidin-1-yl)phenyl)furan-2-carboxamide], a positron-emitting, high-affinity ligand that is specific for the macrophage colony-stimulating factor 1 receptor (CSF1R), the expression of which is essentially restricted to microglia within brain. [^{11}C]CPPC demonstrates high and specific brain uptake in a murine and nonhuman primate lipopolysaccharide model of neuroinflammation. It also shows specific and elevated uptake in a murine model of AD, experimental allergic encephalomyelitis murine model of demyelination and in postmortem brain tissue of patients with AD. Radiation dosimetry in mice indicated [^{11}C]CPPC to be safe for future human studies. [^{11}C]CPPC can be synthesized in sufficient radiochemical yield, purity, and specific radioactivity and possesses binding specificity in relevant models that indicate potential for human PET imaging of CSF1R and the microglial component of neuroinflammation.

neuroinflammation | positron-emission tomography | CSF1R | DAM | [^{11}C]CPPC

PET is the most advanced method by which to quantify brain receptors and their occupancy by endogenous ligands or drugs in vivo. PET imaging of putative neuroinflammatory states (1) has been attempted using radioligands that target the translocator protein (TSPO), which reports on reactive glial cells. Due to limitations of TSPO-targeted PET, including a lack of cell type specificity and sensitivity to genotype, researchers have developed PET radiotracers targeting other aspects of neuroinflammation (P2X7, COX-2, CB2, ROS, A2AR, MMP) [see reviews (2, 3)]. Nevertheless, newer imaging targets, such as P2X7 receptor, are likewise fraught with limitations, including lack of cell-specific expression (*SI Appendix*, Fig. S1). An agent that targets only reactive microglia, which represent up to 10% of cells within the brain (4), might provide a more specific and less ambiguous readout of neuroinflammatory states by imaging this cellular mediator of injury and repair within the CNS.

Within the brain the macrophage colony-stimulating factor 1 receptor (CSF1R) (also known as c-FMS, CD-115, or M-CSFR) is mainly expressed by microglia, while its expression in other cells including neurons is low (5, 6) (*SI Appendix*, Fig. S1). CSF1R is a cell surface protein in a subfamily of tyrosine kinase receptors activated by two homodimeric ligands, CSF1 and IL-34 (7). CSF1R is the primary regulator of the survival, proliferation, differentiation, and function of hematopoietic precursor cells (8). CSF1R directly controls the development, survival, and maintenance of microglia and plays a pivotal role in neuroinflammation (9–13). Inhibition of CSF1R has been pursued as a way to treat a variety of inflammatory and neuroinflammatory disorders (14). Regional distribution of CSF1R in the healthy mammalian brain has not been studied in detail, but expression analysis in mice has demonstrated enhanced levels of CSF1R in superior cortical regions and lower levels in other regions of the brain (15).

Several reports demonstrated up-regulation of CSF1R and CSF1 in the postmortem brain in Alzheimer's disease (AD) (5, 11, 15). Studies in mice showed moderate expression of CSF1R in control brain and high expression in microglia located near amyloid beta (Aβ) deposits in transgenic mouse models of AD (16–18). The gene encoding the cognate ligand for CSF1R, *CSF1*, is up-regulated in stage 2 disease-associated microglia (DAM), which may play a salutary role in keeping AD in check

Significance

[^{11}C]CPPC [5-cyano-*N*-(4-(4-[^{11}C]methylpiperazin-1-yl)-2-(piperidin-1-yl)phenyl)furan-2-carboxamide] is a PET radiotracer specific for CSF1R, a microglia-specific marker. This compound can be used as a noninvasive tool for imaging of reactive microglia, disease-associated microglia and their contribution to neuroinflammation in vivo. Neuroinflammation is posited to be an underlying pathogenic feature of a wide variety of neuropsychiatric disorders. [^{11}C]CPPC may also be used to study specifically the immune environment of malignancies of the central nervous system and to monitor potential adverse neuroinflammatory effects of immunotherapy for peripheral malignancies. This PET agent will be valuable in the development of new therapeutics for neuroinflammation, particularly those targeting CSF1R, not only by providing a noninvasive, repeatable readout in patients but also by enabling measurement of drug target engagement.

Author contributions: A.G.H. and M.G.P. designed research; A.G.H., R.N., C.A.F., I.M., V.M., Y.D., W.B.M., Y. Wu, A.H., C.L., H.-H.A., H.N., W.G.L., H.V., O.P., M.D.S., R.F.D., and M.V.P. performed research; A.G.H., C.A.F., I.M., Y.D., O.P., J.C.T., P.A.C., A.V.S., M.V.P., and M.G.P. contributed new reagents/analytic tools; A.G.H., C.A.F., I.M., Y.D., Y. Wang, W.G.L., O.P., and M.G.P. analyzed data; and A.G.H., C.A.F., I.M., Y.D., W.G.L., and M.G.P. wrote the paper.

The authors declare no conflict of interest.

This article is a PNAS Direct Submission. J.S.L. is a guest editor invited by the Editorial Board.

[1]To whom correspondence may be addressed. Email: ahorti1@jhmi.edu or mpomper@jhmi.edu.

This article contains supporting information online at www.pnas.org/lookup/suppl/doi:10.1073/pnas.1812155116/-/DCSupplemental.

Published online January 11, 2019.

(19, 20). Traumatic brain injury in rodents led to a high and specific increase in CSF1R levels in injured regions (21). CSF1R is altered in lesions due to multiple sclerosis (22). Up-regulated CSF1R was demonstrated in brain tumors (23). HIV-associated cognitive impairment correlated with levels of CSF1R (24). Those properties suggest CSF1R as a viable target for imaging inflammation in general and neuroinflammation specifically. Clinical PET imaging of CSF1R could advance understanding of the CSF1R pathway relevant to neuroinflammation in CNS disorders and guide development of new antiinflammatory CSF1R therapies. Suitable PET radiotracers for imaging of CSF1R are not available. To our knowledge, the only published radiolabeled CSF1R inhibitor was synthesized in 2014 (25), but imaging studies with this radiotracer have not been presented.

The potent and selective CSF1R inhibitor, 5-cyano-*N*-(4-(4-methylpiperazin-1-yl)-2-(piperidin-1-yl)phenyl)furan-2-carboxamide, was developed by the pharmaceutical industry (26). Here, we describe radiosynthesis of its isotopolog, 5-cyano-*N*-(4-(4-[^{11}C]methylpiperazin-1-yl)-2-(piperidin-1-yl)phenyl)furan-2-carboxamide ([^{11}C]CPPC), and evaluation of [^{11}C]CPPC for PET imaging of CSF1R in neuroinflammation.

Materials and Methods

See *SI Appendix* for detailed methods.

Chemistry. CSF1R inhibitors BLZ945 (27) and pexidartinib (PLX3397) (28) were obtained commercially, and compound 8 was prepared in-house as described previously (26). The synthesis of CPPC [5-cyano-*N*-(4-(4-methylpiperazin-1-yl)-2-(piperidin-1-yl)phenyl)furan-2-carboxamide] was performed as described previously (26) and the nor-methyl precursor for radiolabeling of [^{11}C]CPPC, 5-cyano-*N*-(4-(piperazin-1-yl)-2-(piperidin-1-yl)phenyl)furan-2-carboxamide (Pre-CPPC), was prepared similarly (*SI Appendix, Chemistry* and Fig. S2). [^{11}C]CPPC was prepared by reaction of [^{11}C]CH_3I with Pre-CPPC (*SI Appendix, Chemistry* and Fig. S3).

Biodistribution and PET Imaging Studies with [^{11}C]CPPC in Animals. Animal protocols were approved by the Animal Care and Use Committee of the Johns Hopkins Medical Institutions.

Animals. C57BL/6J mice (22–27 g) or CD-1 mice (25–27 g) from Charles River Laboratories served as controls. Microglia-depleted mice were obtained as described previously (10). CSF1R KO (B6.Cg-Csf1r$^{tm1.2Jwp}$/J) mice were purchased from Jackson Laboratories. A mouse model of AD-related amyloidosis-overexpressing Amyloid Precursor Protein with Swedish and Indiana mutations was prepared in-house (29). Male CD-1 mice were injected intracranially (30) with LPS (5 μg; right forebrain) as an intracranial LPS model of neuroinflammation (i.c.-LPS). An i.p. model of neuroinflammation (i.p.-LPS) was generated by injecting male CD-1 mice with LPS (10 mg/kg; 0.2 mL; i.p.) as described previously (31). For the Experimental Autoimmune Encephalitis (EAE) mouse model, female C57BL/6J mice were inoculated with $MOG_{35–55}$ peptide, as described previously (32). Symptomatic MOG-inoculated mice and an uninoculated, healthy mouse were scanned 14 d after the first inoculation.

[^{11}C]CPPC Brain Regional Biodistribution in Mice. The outcome of mouse experiments was calculated as percentage of standardized uptake value (% SUV) or %SUV corrected for radioactivity concentration in blood (SUVR): $SUVR = \%SUV\ tissue / \%SUV\ blood$.

Baseline. Control mice were killed by cervical dislocation at various time points following injection of 5.6 MBq (0.15 mCi) [^{11}C]CPPC in 0.2 mL of saline into a lateral tail vein. The brains were removed and dissected on ice. Various brain regions were weighed, and their radioactivity content was determined in a γ counter. All other mouse biodistribution studies were performed similarly.

Blocking. Mice (male CD1 or C57BL/6J) were killed by cervical dislocation at 45 min following i.v. injection of [^{11}C]CPPC. The blockers, CPPC (0.3, 0.6, 1.2, 3.0, 10, and 20 mg/kg), or CSF1R inhibitor, compound 8 (26) (2 mg/kg), were given i.p., 5 min before [^{11}C]CPPC, whereas baseline animals received vehicle. The brains were removed and dissected on ice, and blood samples were taken from the heart. Regional brain uptake of [^{11}C]CPPC at baseline was compared with that with blocking.

Biodistribution studies in mouse neuroinflammation models (LPS-treated, AD). These studies were performed similarly to the baseline and blocking experiments in control mice.

Determination of CSF1R levels in brains of control and LPS-treated mice. The levels of *Csf1r* mRNA and CSF1R protein were measured by qRT-PCR and Western blot analyses, respectively (*SI Appendix, Materials and Methods* and Fig. S8).

PET/CT Imaging in EAE Mice. Each mouse (three EAE and one control) was injected i.v. with [^{11}C]CPPC, followed by imaging with a PET/CT scanner. PET and CT data were reconstructed using the manufacturer's software and displayed using a medical imaging data analysis (AMIDE) software (amide.sourceforge.net/). To preserve dynamic range, Harderian and salivary gland PET signal was partially masked.

Whole-Body Radiation Dosimetry in Mice. Male CD-1 mice were injected with [^{11}C]CPPC as described above for baseline studies and were euthanized at 10, 30, 45, 60, and 90 min after treatment. The various organs were quickly removed and percentage injected dose (%ID) per organ was determined. The human radiation dosimetry of [^{11}C]CPPC was extrapolated from the mouse biodistribution data using SAAM II (Simulation Analysis and Modeling II) and OLINDA/EXM software. The data were analyzed commercially (RADAR, Inc).

Baboon PET Studies with [^{11}C]CPPC. Three 90-min dynamic PET scans (first: baseline; second: baseline after LPS treatment; third: LPS treatment-plus-blocking) were performed on a male baboon (*Papio Anubis*; 25 kg) using the High Resolution Research Tomograph (CPS Innovations, Inc.). In brief, all PET scans were performed with an i.v. injection of 444–703 MBq (12–19 mCi) [^{11}C]CPPC [specific radioactivity: 1,096–1,184 GBq/μmol (29.6–32.0 Ci/μmol)]. In the LPS scans, the baboon was injected i.v. with 0.05 mg/kg LPS 4 h before the radiotracer. In the LPS-plus-blocking scan, the selective CSF1R inhibitor CPPC (1 mg/kg) was given s.c. 1.5 h before the radiotracer. Changes in the serum level of cytokine IL-6 were monitored with ELISA (*SI Appendix*, Fig. S8). PET data analysis and radiometabolite analysis of baboon arterial blood are described in detail in *SI Appendix*.

Postmortem Human Brain Autoradiography. Use of human tissues has been approved by the Institutional Review Board of the Johns Hopkins Medical Institutions. Slices of inferior parietal cortex (20 μm) of three human subjects suffering from AD and one healthy control (see *SI Appendix*, Table S5 for demographics) on glass slides were used for in vitro autoradiography. The baseline slides were probed with [^{11}C]CPPC, while blocking slides were probed with [^{11}C]CPPC plus blocker (CPPC, BLZ945, pexidartinib, or compound 8) to test CSF1R-binding specificity. The slides were exposed to X-ray film and analyzed with outcome expressed as pmol/mm^3 of wet tissue ± SD.

Results

Chemistry. The precursor for radiolabeling, Pre-CPPC, was prepared in four steps with an overall yield of 54% (*SI Appendix, Chemistry* and Fig. S2) in multimilligram amounts. Radiotracer [^{11}C]CPPC was prepared in a non–decay-corrected radiochemical yield of 21 ± 8% (n = 17), radiochemical purity > 95%, and specific radioactivity at the end-of-synthesis of 977 ± 451 GBq/μmol (26.4 ± 12.2 Ci/μmol) (*SI Appendix*, Fig. S3).

Regional Brain Biodistribution Studies in Control Mice. The regional brain uptake of [^{11}C]CPPC at various time points after injection of radiotracer is shown in *SI Appendix*, Tables S1 and S2. A peak uptake value of 150%SUV was seen in the frontal cortex in 5–15 min after radiotracer injection. Between 30 and 60 min, which encompasses the 45-min time point of several studies described below, changes in %SUV were stable.

Evaluation of Specific Binding of [^{11}C]CPPC in Control Mice. ***Blocking study.*** The blocking of [^{11}C]CPPC uptake was initially performed with escalating doses of nonradiolabeled CPPC (0.6–20 mg/kg). The study showed no reduction of the radiotracer %SUV uptake at low doses and a gradual trend toward increased uptake at high doses (*SI Appendix*, Fig. S4). However, when brain uptake was corrected for the blood input function as SUVR, a significant blocking effect with 20% reduction of radioactivity was observed (*SI Appendix*, Fig. S5).

Comparison of normal control mice vs. microglia-depleted mice. The study showed a small (14%), but significant, reduction in radiotracer uptake in microglia-depleted mouse brain (*SI Appendix*, Fig. S6*A*).

Comparison of normal control mice vs. CSF1R KO mice. The study demonstrated comparable brain uptake (%SUV) of [^{11}C]CPPC in the KO mouse brain vs. controls (*SI Appendix*, Fig. S6*B*).

Biodistribution of [^{11}C]CPPC in LPS-Induced Murine Models of Neuroinflammation. These studies were performed in two murine LPS-induced neuroinflammation models: intracranial LPS (i.c.-LPS) (30) and i.p. LPS (i.p.-LPS) (31, 33). Initially, we examined the induction of CSF1R expression in the brain of i.p.-LPS mice and found a twofold increase of *Csf1r* mRNA and a sixfold increase of the protein by qRT-PCR and Western blot analyses, respectively (*SI Appendix*, Fig. S8).

i.c.-LPS mice. Two independent experiments were performed (Fig. 1). In both experiments, the increase in %SUV in the LPS mice relative to sham mice was significant, and it was higher in the ipsilateral hemisphere than that in the contralateral hemisphere. The greatest increase was observed in the ipsilateral frontal quadrant (53%), where LPS was injected (Fig. 1*B*). The blockade of [^{11}C]CPPC with nonradiolabeled CPPC was dose-dependent. The reduction of uptake in the first experiment was insignificant when a low dose of blocker (0.3 mg/kg) (Fig. 1*A*) was used. The higher doses of blocker (0.6 or 1.2 mg/kg) significantly reduced the uptake of [^{11}C]CPPC in the LPS-treated animals (Fig. 1*B*).

i.p.-LPS mice. Three independent experiments were performed. In the first experiment in the i.p.-LPS mice, [^{11}C]CPPC manifested increased %SUV brain uptake (55%) relative to control animals, but the blocking with nonradiolabeled CPPC did not cause a significant reduction of the %SUV radioactivity in the LPS animals (Fig. 2*A*). In the second and third experiments, the %SUV uptake was corrected for blood radioactivity as SUVR (Fig. 2 *B* and *C*). The SUVR uptake was significantly greater in the i.p.-LPS mice than controls. Blocking with two different CSF1R inhibitors, CPPC (Fig. 2*B*) and compound 8 (Fig. 2*C*), significantly decreased the uptake to the control level. Blood radioactivity concentration changed in the i.p.-LPS baseline (14% reduction) and i.p.-LPS blocking experiments (39% increase) vs. controls.

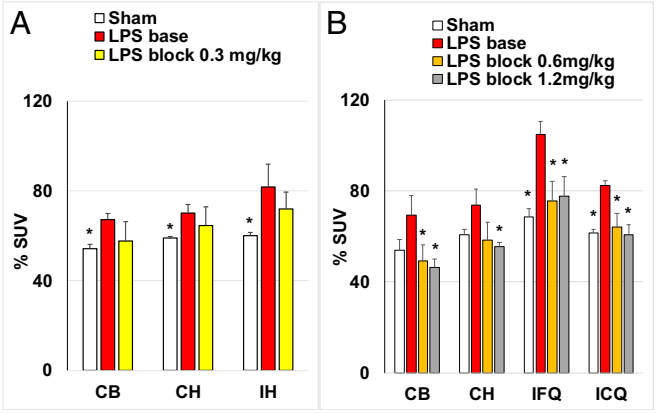

Fig. 1. Comparison of [^{11}C]CPPC brain uptake in sham and LPS: right forebrain injected mice, baseline, and blocking. Two independent experiments (*A* and *B*) were performed. The time point was 45 min after radiotracer injection; LPS (5 μg in 0.5 μL) or saline (0.5 μL) was injected into the right forebrain (ipsilateral frontal quadrant) 2–3 d before the radiotracer study. Blocker (CPPC) was injected i.p. 5 min before the radiotracer. (*A*) The regions of interest (ROIs) are cerebellum (CB), ipsilateral hemisphere (IH), and contralateral hemisphere (CH). The data are mean %SUV ± SD (n = 3). (*B*) The ROIs are cerebellum (CB), contralateral hemisphere (CH), ipsilateral caudal quadrant (ICQ), and ipsilateral frontal quadrant (IFQ). The data are mean %SUV ± SD (n = 4). Statistical analysis: comparison of LPS-baseline versus sham or LPS-block. *P < 0.05; no asterisk indicates P > 0.05 (ANOVA).

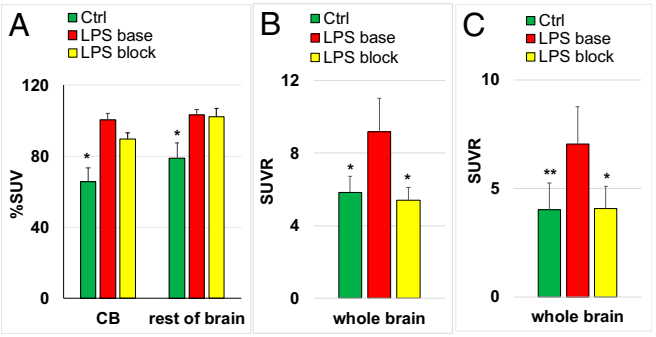

Fig. 2. Brain uptake of CSF1R radiotracer [^{11}C]CPPC in control (Ctrl), LPS (i.p.)-treated mice (LPS base), and LPS (i.p.)-treated mice plus blocking with CSF1R inhibitors (LPS block) in three independent experiments. The time point was 45 min after radiotracer injection [LPS (10 mg/kg)]. (*A*) Data are mean %SUV ± SD (n = 5). CB, cerebellum. (*B*) Data are mean SUVR ± SD (n = 5). Blocker (CPPC, 1 mg/kg, i.p.) was injected in the LPS-treated mice. (*C*) Data are mean SUVR ± SD (n = 3–6). Blocker (compound 8, 2 mg/kg, i.p.) was injected in the LPS-treated mice. Statistical analysis: comparison of LPS-baseline versus control or LPS-block. *P < 0.01; **P = 0.03; no asterisk indicates P > 0.05 (ANOVA).

Brain Regional Distribution of [^{11}C]CPPC in a Transgenic Mouse Model of AD. [^{11}C]CPPC uptake was significantly higher in all brain regions of AD mice with greatest increase (31%) in the cortex (Fig. 3).

Whole-Body Radiation Dosimetry in Mice. Most organs received 0.002–0.006 mSv/MBq [0.007–0.011 Roentgen equivalent man (Rem)/mCi]. The small intestine received the highest dose of 0.047 mSv/MBq (0.17 Rem/mCi). The effective dose was 0.0048 mSv/MBq (0.018 Rem/mCi) (*SI Appendix*, Table S3).

[^{11}C]CPPC PET/CT in the Murine EAE Model of Multiple Sclerosis. Three mice representing a spectrum of EAE severity (EAE scores of 0.5, 2.5, and 4.5) and a single healthy mouse receiving no antigen or adjuvant were injected with [^{11}C]CPPC and dynamically scanned using PET/CT (Fig. 4). The maximum intensity projection (MIP) images and sagittal slices of each mouse (Fig. 4*A*) show the radiotracer uptake intensity that correlates with disease severity with greatest increase (99%) in the brainstem (Fig. 4*B*), while muscle uptake was comparable between mice. The raw images without Harderian and salivary gland thresholding are shown in *SI Appendix*, Fig. S7.

PET in Baboon. Comparison of the dynamic PET [^{11}C]CPPC scans in the same baboon in baseline, LPS, and LPS-plus-block experiments demonstrated an increase of parametric volume of distribution (V_T) after LPS treatment and reduction to the baseline level of the V_T after LPS-plus-blocking treatment (Fig. 5 and *SI Appendix*, Fig. S9). Serum levels of IL-6 strongly increased after the administration of LPS, suggesting successful induction of acute inflammation (*SI Appendix*, Fig. S10).

Dynamic [^{11}C]CPPC PET baseline imaging in a baboon showed accumulation of radioactivity in the brain with a peak SUV of 2.5–4.0 at 20 min postinjection, followed by gradual decline (Fig. 5*B*). Regional V_T was moderately heterogeneous, highest in the putamen, caudate, thalamus, and insula; intermediate in the frontal cortex; and lowest in the cerebellum, hypothalamus, and occipital cortex (Fig. 5*A* and *SI Appendix*, Fig. S9).

Comparison of baboon PET at baseline vs. LPS vs. LPS-plus-blocking showed a small difference in SUV within brain. However, the washout rate in the baseline scan was more rapid than that in the LPS scan (Fig. 5*C*).

Radiometabolite analysis of blood samples from baboons showed that [^{11}C]CPPC was metabolized to two radiometabolites (71–76% total radiometabolites) at 90 min postinjection (*SI Appendix*, Fig. S11). Those hydrophilic radiometabolites entered the brain minimally, as demonstrated in mouse experiments. Analysis

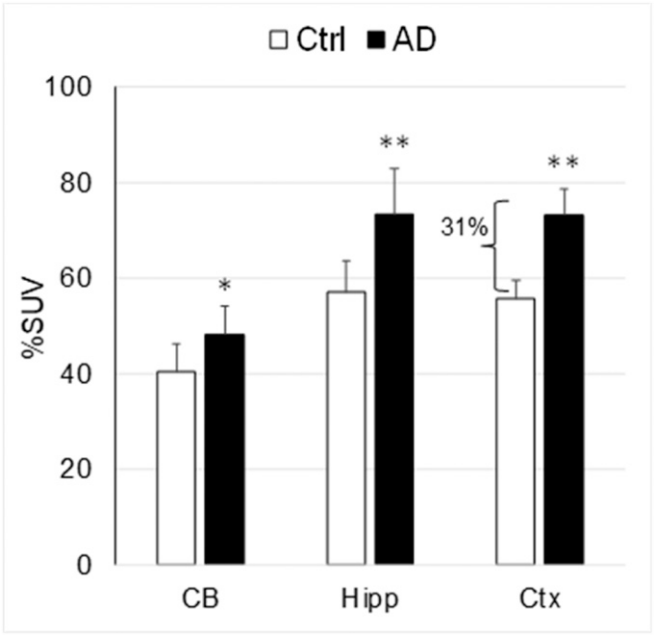

Fig. 3. Comparison of the [^{11}C]CPPC brain uptake in transgenic AD (n = 6) and control (n = 5) mice. Time-point – 45 min after radiotracer injection. Data: mean %SUV ± SD. *P = 0.04, **P < 0.005 (ANOVA). The uptake of [^{11}C]CPPC was significantly greater in AD mouse brain regions. CB, cerebellum; Ctx, cortex; Hipp, hippocampus.

by HPLC showed that at least 95% of the radioactivity in the mouse brain was the parent [^{11}C]CPPC (*SI Appendix*, Table S4).

Metabolite-corrected [^{11}C]CPPC radioactivity in baboon plasma greatly decreased (~50%) in the LPS-treated vs. baseline, with recovery to baseline levels in the LPS-plus-blocking experiment (Fig. 5*D*). Mathematical modeling using compartmental and Logan analysis (*SI Appendix*, Fig. S12) demonstrated a dramatic increase (90–120%) of parametric V_T values in the LPS-treated baboon (V_T = 35–52) vs. baseline (V_T = 15–25), with a return to the baseline level in the LPS-plus-blocking study (Fig. 5 and *SI Appendix*, Fig. S9), whereas the K_1 value changed only slightly (*SI Appendix*, Fig. S13). The increase of radiotracer binding in the LPS-treated baboon brain was CSF1R-specific, as demonstrated on the blocking scan.

Postmortem Autoradiography of [^{11}C]CPPC in Human Brain. The comparison of [^{11}C]CPPC baseline autoradiography in the AD vs. control brain slices (Fig. 6 and *SI Appendix*, Table S6) showed an increase (75–99%) of radiotracer binding in the AD brain. The binding specificity was tested by comparing the baseline binding with binding in blocking experiments using four different CSF1R inhibitors. The baseline/blocking ratio in the AD brain was 1.7–2.7 (blocker: CPPC), whereas in the control brain the ratio was 1.4 (Fig. 6 and *SI Appendix*, Table S6). When other CSF1R blockers (compound 8, BLZ945, and PLX3397) were used in the same AD brains, the baseline/blocking ratios were 2.0 ± 0.23, 1.79 ± 0.88, and 1.25 ± 0.25, respectively (*SI Appendix*, Fig. S14).

Discussion

We have developed a PET radiotracer specific for CSF1R in vitro in human brain tissue and in vivo in nonhuman primate and murine models of neuroinflammation. While we and others [see reviews (2, 3)] have worked to develop and implement PET biomarkers for neuroinflammation, none has proved selective to microglia, the resident immune cells of the brain, until [^{11}C]CPPC.

The lead CSF1R inhibitor for development of [^{11}C]CPPC was selected from the literature (26). Original, nonradiolabeled CPPC exhibited high CSF1R inhibitory potency [IC_{50} = 0.8 nM (26)] and suitable physical properties for brain PET, including optimal lipophilicity with a calculated partition coefficient ($clogD_{7.4}$) of 1.6 and molecular mass of 393 Da, which portend blood–brain barrier permeability. [^{11}C]CPPC was prepared in suitable radiochemical yield with high purity and specific radioactivity (*SI Appendix*, Fig. S3).

Biodistribution and Specific Binding of [^{11}C]CPPC Studies in Control Mice. Brain uptake of [^{11}C]CPPC in control mice was robust, with a peak of 150%SUV or 6.4%ID/g tissue in frontal cortex, followed by a decline (*SI Appendix*, Table S2). The regional brain distribution was moderately heterogeneous, with the highest accumulation of radioactivity in frontal cortex, in agreement with analysis of CSF1R expression in normal mouse brain (34). Among brain regions studied here, the brainstem and cerebellum showed the lowest accumulation of [^{11}C]CPPC.

CSF1R binding specificity of [^{11}C]CPPC in normal mouse brain was evaluated using three approaches: comparison of baseline controls with (*i*) blocking, (*ii*) microglia-depleted, and (*iii*) CSF1R KO mice. The initial dose–escalation blocking study in normal mouse brain failed to show a significant reduction of %SUV (*SI Appendix*, Figs. S3 and S4*A*). However, when the %SUV was corrected for radioactivity in the blood as SUVR, a moderate, but significant, reduction (20%) was observed (*SI Appendix*, Fig. S4*B*), demonstrating that [^{11}C]CPPC specifically labels CSF1R in normal mouse brain. That [^{11}C]CPPC concentration in blood was greater in the blocking studies is also noteworthy.

Chronic treatment of mice with the CSF1R inhibitor PLX3397 (pexidartinib) effectively depletes microglia (90%) and reduces CSF1R in the animal brain (10). Brain uptake of [^{11}C]CPPC in the microglia-depleted mice was lower (14%) than in controls (*SI Appendix*, Fig. S6*A*). That reduced uptake may be due to a combination of two effects, namely, depletion of microglia and the blocking effect of PLX3397 per se. Finally, the comparison of [^{11}C]CPPC uptake in the control and CSF1R KO mice showed comparable radiotracer uptake to the control and KO mice (*SI Appendix*, Fig. S6*B*). While depleted (PLX3397) or absent (KO) CSF1R target indicates that there should be little to no brain uptake of a CSF1R-specific imaging agent, there is only modest expression of CSF1R in healthy rodent brain (34–36), necessitating attention to relevant animal models where CSF1R would be present in higher amounts.

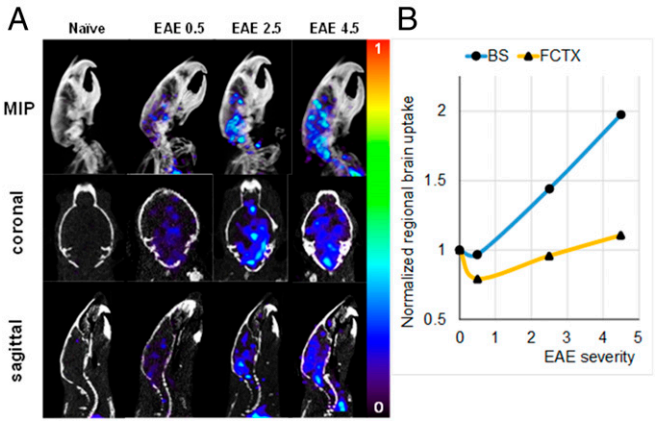

Fig. 4. [^{11}C]CPPC PET/CT imaging in murine EAE. (*A*) MIP (*Top*), coronal (*Middle*), and sagittal (*Bottom*) slices showing radiotracer uptake from 45 to 60 min per projection in the indicated mice. Color scale range shows %ID/g tissue. (*B*) Regional brain uptake normalized by uptake in control animal vs. EAE severity. BS, brainstem; FCTX, frontal cortex.

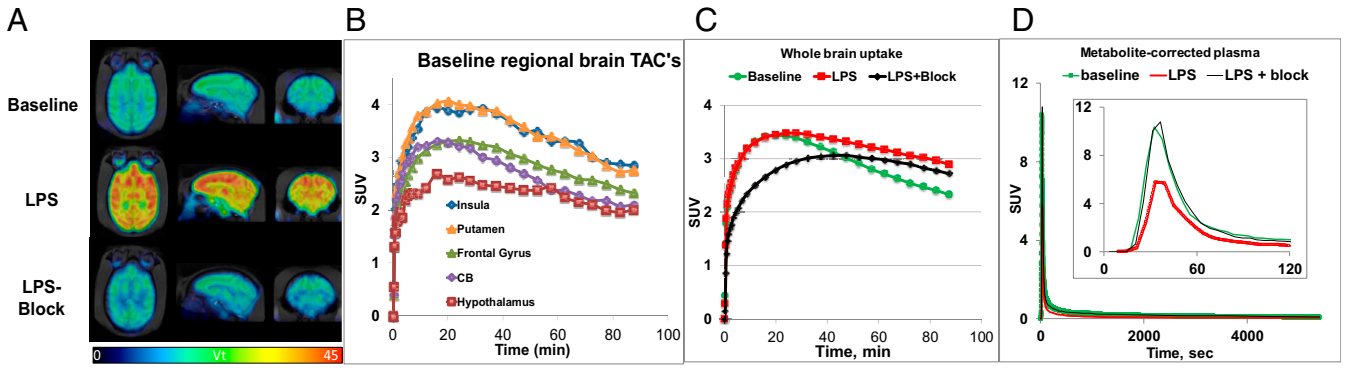

Fig. 5. PET imaging of [^{11}C]CPPC in the same baboon in baseline, LPS, and LPS-plus-blocking experiments. The LPS dose was 0.05 mg/kg (i.v.), 4 h before radiotracer injection. (*A*) Parametric (V_T) images. (*B*) Baseline regional brain SUV time-uptake curves of [^{11}C]CPPC. (*C*) Whole-brain SUV time-uptake curves of [^{11}C]CPPC: baseline (green), after LPS treatment (red) and blocking after LPS treatment (black). (*D*) Metabolite-corrected plasma SUV time-uptake curves of [^{11}C]CPPC: baseline (green), after LPS treatment (red), and LPS-plus-blocking (black). The *Inset* in *D* shows first 120 s of scanning.

Evaluation of [^{11}C]CPPC in Murine Models of LPS-Induced Neuroinflammation. LPS stimulation is a common model of neuroinflammation (31, 33). LPS-induced neuroinflammation was used for testing various PET radiotracers in rodents, nonhuman primates, and even human subjects [see review (2)]. Reports describing CSF1R expression in LPS neuroinflammation models are not available. We compared the CSF1R levels in the brain of the i.p.-LPS mice vs. control mice using qRT-PCR and Western blot and found a high increase of *Csf1r* mRNA and CSF1R protein expression (*SI Appendix*, Fig. S8). In this study, two murine models of LPS-induced neuroinflammation, i.c.-LPS (30, 37) and i.p.-LPS (31, 33), were used. Even though stereotactic surgery may damage the blood–brain barrier in the i.c-LPS animals, this model, which produces localized neuroinflammation, initially appeared more attractive than the i.p-LPS model with diffused neuroinflammation. However, further studies with [^{11}C]CPPC showed comparable results using both models.

[^{11}C]CPPC-binding experiments demonstrated a significant elevation (up to 53%) of uptake in i.c.-LPS mice (Fig. 1). The elevated binding was ∼50% specific vs. sham animals and mediated through CSF1R, as demonstrated in the dose-escalation blocking experiments (Fig. 1). In the i.p.-LPS mice, [^{11}C]CPPC binding was also significantly higher (up to 55–59%) vs. control animals (Fig. 2). Whole-brain [^{11}C]CPPC binding in the i.p.-LPS mice was more than 50% specific and mediated through CSF1R, as demonstrated in blocking experiments using two different CSF1R inhibitors, CPPC (Fig. 2*B*) and compound 8 (Fig. 2*C*). In the i.p.-LPS animals, the blood radioactivity concentration changed dramatically, necessitating the correction of %SUV for the blood input function as SUVR (Fig. 2 *B* and *C*). The blood radioactivity changes may be explained by unavoidable systemic changes of CSF1R levels in the i.p.-LPS mice. The [^{11}C]CPPC studies in the intracranial and i.p. murine LPS models showed comparable results demonstrating that the radiotracer specifically labels CSF1R in both models. The ex vivo binding potential ($BP_{ex\ vivo}$ = 0.53–0.62) of [^{11}C]CPPC in the LPS mice was estimated as LPS uptake − sham uptake/sham uptake. A previous study in LPS-treated rats with the TSPO radiotracer [^{11}C]PK11195 gave a comparable BP value of 0.47 (38).

[^{11}C]CPPC Imaging of EAE Mice. PET/CT imaging in the C57BL/6 $MOG_{35–55}$ EAE model showed that the PET signal intensity was proportional to disease score (Fig. 4) and largely concentrated in the brainstem, cerebellum, and cervical spine, in agreement with the regional distribution of demyelination in the EAE model. The brainstem uptake of [^{11}C]CPPC was up to twofold greater in the EAE mice vs. control animals.

Whole-Body Radiation Dosimetry in Mice. Dosimetry was performed for future translation of [^{11}C]CPPC to humans. The mouse study demonstrated that a proposed dose of 740 MBq (20 mCi) [^{11}C]CPPC administered to a human subject would result in a radiation burden below the current Food and Drug Administration limit (5 Rem; (39)), but an actual study in human subjects is needed to confirm this estimate.

PET Imaging in Baboon. Systemic administration of LPS to baboon causes microglial activation (40). In this report, we tested binding properties of [^{11}C]CPPC in a control baboon and in the same baboon injected with a low dose of LPS (0.05 mg/kg, i.v.). We observed more than a twofold increase of distribution volume (V_T) values in all brain regions of the LPS-treated animal (Fig. 5 and *SI Appendix*, Fig. S9). The increase of parametric V_T in the LPS-baboon was fully blocked by injection of nonradiolabeled CPPC (Fig. 5*A* and *SI Appendix*, Fig. S9). The parametric modeling of those images is essential because injection of LPS and blocker cause changes in the blood input function (Fig. 5*D*), most likely due to CSF1R changes in the periphery. Parametric modeling did not require inclusion of brain radiometabolites, because HPLC analysis showed mostly unchanged parent [^{11}C]CPPC in the animal brain (>95%).

[^{11}C]CPPC PET scans demonstrated that radiotracer binding in the LPS-treated baboon brain was specific and mediated by CSF1R, rendering this agent suitable for imaging of neuroinflammation in nonhuman primates. The increase of [^{11}C]CPPC V_T (85–120%) in the baboon treated with LPS (0.05 mg/kg) was

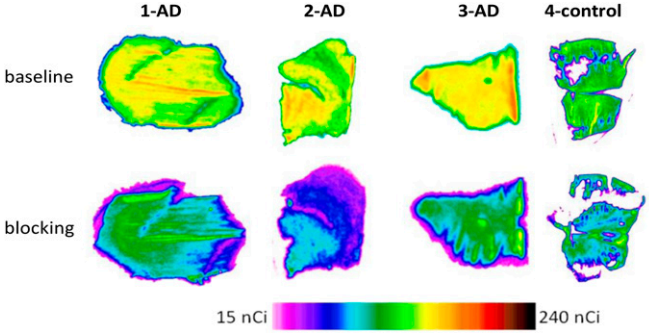

Fig. 6. Postmortem human autoradiography/[^{11}C]CPPC images (baseline and blocking) in inferior parietal lobe gray matter slices. Three subjects with Alzheimer's disease (1-AD, 2-AD, and 3-AD) and control (4-control) subject. See also *SI Appendix*, Fig. S14 and Tables S5 and S6.

at least the same or higher than that for the TSPO radiotracer [^{11}C]PBR28 (range, 35.6–100.7%) in response to a greater dose of LPS (0.1 mg/kg), as shown in a previous report (40). Accordingly, [^{11}C]CPPC might provide an innovative tool with high sensitivity for quantitative imaging of activated microglia in neuroinflammation.

[^{11}C]CPPC Binding in AD Brain. There is an immune component to AD, particularly involving the innate immune system, which is different from "typical" neuroinflammatory diseases, such as multiple sclerosis or several of the models described above (41). Previous research provided evidence of up-regulation of CSF1R in the brains of human subjects suffering from AD (5, 11, 15) and in transgenic mouse models of AD (16–18). We tested the binding of [^{11}C]CPPC in transgenic AD mouse brain and in postmortem AD human brain tissue. In agreement with previous data (16–18), the ex vivo brain uptake of [^{11}C]CPPC in transgenic AD mice was significantly higher (up to 31%) than that in control animals (Fig. 3).

Postmortem human in vitro autoradiography showed that [^{11}C]CPPC specifically labeled CSF1R in the AD brain (baseline/self-blocking ratio up to 2.7) (Fig. 6 and *SI Appendix*, Table S6). In a separate experiment, CSF1R inhibitors, structurally different from CPPC [compound 8, IC_{50} = 0.8 nM (26); BLZ945, IC_{50} = 1.2 nM (27); and PLX3397, IC_{50} = 20 nM (28)], blocked [^{11}C]CPPC binding in the same AD tissue (*SI Appendix*, Fig. S14), confirming that binding was CSF1R-specific (Fig. 6 and *SI Appendix*, Fig. S14 and Table S6). The baseline/blocking ratios for more potent CSF1R inhibitors, namely, compound 8 and BLZ945, were up to two times greater than that of less potent PLX3397. Those findings may be extended to imaging other neurodegenerative disorders or conditions with an innate immune component, such as amyotrophic lateral sclerosis, aging, or Parkinson's disease (19), which involve DAM. [^{11}C]CPPC may also provide an indirect imaging readout for TREM2 signaling (19, 42), which has not been imaged in vivo.

Conclusion

We have developed [^{11}C]CPPC, a PET radiotracer for imaging CSF1R in neuroinflammation. Specific binding of the radiotracer is increased in mouse (up to 59%) and baboon (up to 120%) models of LPS-induced neuroinflammation, murine models of AD (31%) and multiple sclerosis (up to 100%), and in postmortem AD human brain tissue (base/block ratio of 2.7). Radiation dosimetry studies in mice demonstrated that [^{11}C]CPPC is safe for human studies. [^{11}C]CPPC radiometabolites minimally enter the animal brain, indicating that their inclusion in image analysis is not required. [^{11}C]CPPC is poised for clinical translation to study CSF1R in a variety of clinical scenarios.

ACKNOWLEDGMENTS. We acknowledge Dr. Xiaolei Song for providing an EAE mouse and Dr. Hiroto Kuwabara for fruitful discussions. We are grateful to Dr. Polina Sysa Shah; Paige Finley, MS; and James Engles, MS, for assistance with animal experiments. This research was supported by NIH Grants AG054802, EB024495, and NS041435 and by the Johns Hopkins University Alzheimer's Disease Research Center (Grant AG05146).

1. Masgrau R, Guaza C, Ransohoff RM, Galea E (2017) Should we stop saying 'glia' and 'neuroinflammation'? *Trends Mol Med* 23:486–500.
2. Tronel C, et al. (2017) Molecular targets for PET imaging of activated microglia: The current situation and future expectations. *Int J Mol Sci* 18:E802.
3. Janssen B, Vugts DJ, Windhorst AD, Mach RH (2018) PET imaging of microglial activation-beyond targeting TSPO. *Molecules* 23:607.
4. Aguzzi A, Barres BA, Bennett ML (2013) Microglia: Scapegoat, saboteur, or something else? *Science* 339:156–161.
5. Akiyama H, et al. (1994) Expression of the receptor for macrophage colony stimulating factor by brain microglia and its upregulation in brains of patients with Alzheimer's disease and amyotrophic lateral sclerosis. *Brain Res* 639:171–174.
6. Zhang Y, et al. (2014) An RNA-sequencing transcriptome and splicing database of glia, neurons, and vascular cells of the cerebral cortex. *J Neurosci* 34:11929–11947.
7. Peyraud F, Cousin S, Italiano A (2017) CSF-1R inhibitor development: Current clinical status. *Curr Oncol Rep* 19:70.
8. Chitu V, Gokhan Ş, Nandi S, Mehler MF, Stanley ER (2016) Emerging roles for CSF-1 receptor and its ligands in the nervous system. *Trends Neurosci* 39:378–393.
9. Ginhoux F, et al. (2010) Fate mapping analysis reveals that adult microglia derive from primitive macrophages. *Science* 330:841–845.
10. Elmore MR, et al. (2014) Colony-stimulating factor 1 receptor signaling is necessary for microglia viability, unmasking a microglia progenitor cell in the adult brain. *Neuron* 82:380–397.
11. Walker DG, Tang TM, Lue LF (2017) Studies on colony stimulating factor receptor-1 and ligands colony stimulating factor-1 and interleukin-34 in Alzheimer's disease brains and human microglia. *Front Aging Neurosci* 9:244.
12. Smith AM, et al. (2013) M-CSF increases proliferation and phagocytosis while modulating receptor and transcription factor expression in adult human microglia. *J Neuroinflammation* 10:85.
13. Palle P, Monaghan KL, Milne SM, Wan ECK (2017) Cytokine signaling in multiple sclerosis and its therapeutic applications. *Med Sci (Basel)* 5:E0023.
14. El-Gamal MI, et al. (2018) Recent advances of colony-stimulating factor-1 receptor (CSF-1R) kinase and its inhibitors. *J Med Chem* 61:5450–5466.
15. Lue LF, et al. (2001) Inflammatory repertoire of Alzheimer's disease and nondemented elderly microglia in vitro. *Glia* 35:72–79.
16. Murphy GM, Jr, Zhao F, Yang L, Cordell B (2000) Expression of macrophage colony-stimulating factor receptor is increased in the AbetaPP(V717F) transgenic mouse model of Alzheimer's disease. *Am J Pathol* 157:895–904.
17. Yan SD, et al. (1997) An intracellular protein that binds amyloid-beta peptide and mediates neurotoxicity in Alzheimer's disease. *Nature* 389:689–695.
18. Boissonneault V, et al. (2009) Powerful beneficial effects of macrophage colony-stimulating factor on beta-amyloid deposition and cognitive impairment in Alzheimer's disease. *Brain* 132:1078–1092.
19. Deczkowska A, et al. (2018) Disease-associated microglia: A universal immune sensor of neurodegeneration. *Cell* 173:1073–1081.
20. Keren-Shaul H, et al. (2017) A unique microglia type associated with restricting development of Alzheimer's disease. *Cell* 169:1276–1290.e17.
21. Raivich G, et al. (1998) Regulation of MCSF receptors on microglia in the normal and injured mouse central nervous system: A quantitative immunofluorescence study using confocal laser microscopy. *J Comp Neurol* 395:342–358.
22. Prieto-Morin C, Ayrignac X, Ellie E, Tournier-Lasserve E, Labauge P (2016) CSF1R-related leukoencephalopathy mimicking primary progressive multiple sclerosis. *J Neurol* 263:1864–1865.
23. Alterman RL, Stanley ER (1994) Colony stimulating factor-1 expression in human glioma. *Mol Chem Neuropathol* 21:177–188.
24. Lentz MR, et al. (2010) Exploring the relationship of macrophage colony-stimulating factor levels on neuroaxonal metabolism and cognition during chronic human immunodeficiency virus infection. *J Neurovirol* 16:368–376.
25. Bernard-Gauthier V, Schirrmacher R (2014) 5-(4-((4-[(18)F]Fluorobenzyl)oxy)-3-methoxybenzyl)pyrimidine-2,4-diamine: A selective dual inhibitor for potential PET imaging of Trk/CSF-1R. *Bioorg Med Chem Lett* 24:4784–4790.
26. Illig CR, et al. (2008) Discovery of novel FMS kinase inhibitors as anti-inflammatory agents. *Bioorg Med Chem Lett* 18:1642–1648.
27. Krauser JA, et al. (2015) Phenotypic and metabolic investigation of a CSF-1R kinase receptor inhibitor (BLZ945) and its pharmacologically active metabolite. *Xenobiotica* 45:107–123.
28. DeNardo DG, et al. (2011) Leukocyte complexity predicts breast cancer survival and functionally regulates response to chemotherapy. *Cancer Discov* 1:54–67.
29. Melnikova T, et al. (2013) Reversible pathologic and cognitive phenotypes in an inducible model of Alzheimer-amyloidosis. *J Neurosci* 33:3765–3779.
30. Dobos N, et al. (2012) The role of indoleamine 2,3-dioxygenase in a mouse model of neuroinflammation-induced depression. *J Alzheimers Dis* 28:905–915.
31. Qin L, et al. (2007) Systemic LPS causes chronic neuroinflammation and progressive neurodegeneration. *Glia* 55:453–462.
32. Jones MV, et al. (2008) Behavioral and pathological outcomes in MOG 35-55 experimental autoimmune encephalomyelitis. *J Neuroimmunol* 199:83–93.
33. Catorce MN, Gevorkian G (2016) LPS-induced murine neuroinflammation model: Main features and suitability for pre-clinical assessment of nutraceuticals. *Curr Neuropharmacol* 14:155–164.
34. Nandi S, et al. (2012) The CSF-1 receptor ligands IL-34 and CSF-1 exhibit distinct developmental brain expression patterns and regulate neural progenitor cell maintenance and maturation. *Dev Biol* 367:100–113.
35. Michaelson MD, et al. (1996) CSF-1 deficiency in mice results in abnormal brain development. *Development* 122:2661–2672.
36. Lee SC, et al. (1993) Macrophage colony-stimulating factor in human fetal astrocytes and microglia. Differential regulation by cytokines and lipopolysaccharide, and modulation of class II MHC on microglia. *J Immunol* 150:594–604.
37. Aid S, Parikh N, Palumbo S, Bosetti F (2010) Neuronal overexpression of cyclooxygenase-2 does not alter the neuroinflammatory response during brain innate immune activation. *Neurosci Lett* 478:113–118.
38. Dickens AM, et al. (2014) Detection of microglial activation in an acute model of neuroinflammation using PET and radiotracers 11C-(R)-PK11195 and 18F-GE-180. *J Nucl Med* 55:466–472.
39. 5. *Federal Register* §361.1 (2018), pp 21378–21381.
40. Hannestad J, et al. (2012) Endotoxin-induced systemic inflammation activates microglia: [^{11}C]PBR28 positron emission tomography in nonhuman primates. *Neuroimage* 63:232–239.
41. Heppner FL, Ransohoff RM, Becher B (2015) Immune attack: The role of inflammation in Alzheimer disease. *Nat Rev Neurosci* 16:358–372.
42. Hickman SE, El Khoury J (2014) TREM2 and the neuroimmunology of Alzheimer's disease. *Biochem Pharmacol* 88:495–498.